Inorg. Chem. **2009**, *48*, 565−573

All-*trans*-[ClRu^{II}(py)$_4$(NC)Ru^{II}(py)$_4$(CN)Ru^{II}(py)$_4$(NO)](PF$_6$)$_4$: A Redox-Active 2-Donor/1-Acceptor System Based on the Electrophilic {RuNO}^{6} Motif

Ariel G. De Candia,[†] Priti Singh,[‡] Wolfgang Kaim,[‡] and Leonardo D. Slep*[,†]

Departamento de Química Inorgánica, Analítica y Química Física, INQUIMAE, Facultad de Ciencias Exactas y Naturales Universidad de Buenos Aires, Pabellón 2, Ciudad Universitaria, C1428EHA Buenos Aires, Argentina, and Institut für Anorganische Chemie, Universität Stuttgart, Pfaffenwaldring 55, D-70550 Stuttgart, Germany

Received July 18, 2008

The new linear homotrinuclear compound *trans*-[ClRu^{II}(py)$_4$(NC)Ru^{II}(py)$_4$(CN)Ru^{II}(py)$_4$(NO)](PF$_6$)$_4$ was prepared by reaction between the nitro complex *trans*-[(NC)Ru^{II}(py)$_4$(CN)Ru^{II}(py)$_4$(NO$_2$)]$^+$ and the solvento complex obtained by reaction between [ClRu^{II}(py)$_4$(NO)]$^{3+}$ and N_3^- in acetone. The *trans*-[ClRu^{II}(py)$_4$ (NC)Ru^{II}(py)$_4$(CN)Ru^{II}(py)$_4$(NO)]$^{4+}$ ion (**I**) has been characterized by ^{1}H NMR and IR spectroscopy (ν_{NO} = 1919 cm^{-1}). This species displays intense electronic absorptions in the visible region which can be assigned to donor−acceptor charge-transfer transitions (DACT) involving {RuNO}^{6}-centered acceptor orbitals and donor orbitals located on the two different neighboring metal centers at ca. 6.7 and 12.6 Å distance from the metal in the {RuNO}^{6} fragment. Addition of OH$^-$ to **I** generated the nitro complex with a second-order rate constant of (12.5 ± 0.2) × 10^3 M^{-1} s^{-1} (25 °C). Cyclic voltammetry experiments complemented by spectroelectrochemistry in the UV−vis−NIR region reveal that **I** can be reversibly reduced at 0.49 or 0.20 V vs AgCl/Ag for acetonitrile and water, respectively, and oxidized at 0.71 or 0.57 V vs AgCl/Ag. The spectroscopic and spectroelectrochemical information (UV−vis−NIR, X-band EPR) supplemented with electronic structure computation (DFT) reveals that the one-electron reduction is centered on the nitrosyl moiety to yield a {RuNO}^{7} species, while oxidation occurs on the chlororuthenium side of the molecule. Both processes yield significant changes of the electronic spectra which are discussed in parallel with the electronic structure picture as obtained by DFT.

Introduction

Exploration of oligonuclear cyanide-bridged systems has uncovered several linear M−CN−M′ assemblies with moderate/strong metal−metal interactions and interesting magnetic, photophysical, and electronic properties. Mixed-valent systems of this kind have proven ideal to study long-range donor−acceptor interactions and electron-transfer processes. They also provide maximum charge separation in photophysical processes, making them attractive in construction of light-harvesting devices.[1]

Metal nitrosyl complexes have been known for a long time, leading to a considerable number of well-characterized mononuclear compounds with varying coordination numbers.[2,3] The overall structural and reactivity features of metal nitrosyls have been classically rationalized in terms of the Enemark and Feltham {MNO}^{n} description, where n is the sum of the metal d electrons and nitrosyl π^* electrons.[4] Many of these well-studied species correspond to n = 6 with linear MNO arrangements and an electrophilic reactivity centered at the N atom of the MNO moiety. For species with n = 7 and 8 the reports reveal increasingly bent MNO bonds.[4−6]

Sometime ago[7] we showed that the {MNO}^{6} fragment can be incorporated into a dinuclear species that, apart from preserving the usual nitrosyl features, behaves as a donor−acceptor (D−A) system, similar to the mixed-valent devices described above. Specifically, we reported the preparation and spectroscopic characterization of *trans*-[(NC)Ru^{II}(py)$_4$(CN)Ru^{II}(py)$_4$(NO)]$^{3+}$ and its 1e$^-$ reduced and oxidized forms.[7] This compound displays an intense absorption in the visible region that we attributed to the charge-transfer process involving Ru^{II}(py)$_4$(CN)$_2$ as the donor fragment and [Ru^{II}(py)$_4$(NO)]$^{3+}$ as the acceptor.

* To whom correspondence should be addressed. E-mail: slep@qi.fcen.uba.ar.
† Universidad de Buenos Aires.
‡ Universität Stuttgart.

10.1021/ic801347d CCC: $40.75
Published on Web 12/18/2008

In this work we extend this idea and add another metallic center to the above species to yield the linear homotrinuclear all-*trans*-$[ClRu^{II}(py)_4(NC)Ru^{II}(py)_4(CN)Ru^{II}(py)_4(NO)]^{4+}$ species. We report the preparation, basic characterization, and electronic spectroscopy of this compound, a triad of donor/acceptor fragments that reveals long-distance charge transfer.

Experimental Section

Materials. Complexes $RuCl_2(dmso)_4$, *trans*-$Ru(CN)_2(py)_4$, *trans*-$RuCl_2(py)_4$, *trans*-$[Ru^{II}Cl(py)_4(NO)](PF_6)_2$, and $[(NC)Ru^{II}(py)_4(CN)Ru^{II}(py)_4Cl](PF_6)$ were prepared according to previously published procedures.[7−11] Solvents for UV−vis and electrochemistry measurements were dried according to literature procedures.[12] The tetra-*n*-butylammonium hexafluorophosphate, Bu_4NPF_6 (Aldrich), used in the cyclic voltammetry and spectroelectrochemical experiments was recrystallized from ethanol. All other reagents were obtained commercially and used as supplied. The compounds synthesized in this work were routinely dried in a vacuum desiccator for at least 12 h prior to characterization.

Synthesis of the Compounds. All preparations were performed under argon using standard Schlenk glassware.

***trans*-$[(NC)Ru^{II}(py)_4(CN)Ru^{II}(py)_4(NO_2)](PF_6)$.** A 285 mg (0.27 mmol) amount of $[(NC)Ru^{II}(py)_4(CN)Ru^{II}(py)_4Cl](PF_6)$[8] was suspended in 380 mL of water in the presence of a large excess of $NaNO_2$ (0.95 g, 13.8 mmol). The suspension was stirred in the dark for 48 h, yielding a clear yellow solution. Evaporation to ca. 25 mL induced precipitation of a yellow solid, which was completed by addition of 1 mL of an aqueous saturated solution of NH_4PF_6. The product was collected by filtration, washed with small portions of chilled water, and dried under vacuum. Yield: 216 mg (74%). Anal. Calcd for $C_{42}H_{40}F_6N_{11}O_2PRu_2$ (MW = 1077.94 g mol^{-1}): C, 46.8; H, 3.7; N, 14.3. Found: C, 46.7; H, 3.7; N, 14.4. ^{1}H NMR, δ_H (CD_3CN): 8.28 (8H, d, $H^{2',6'} \times 4$), 8.23 (8H, d, $H^{2,6} \times 4$), 7.83 (4H, t, $H^4 \times 4$), 7.75 (4H, t, $H^{4'} \times 4$), 7.09 (8H, t, $H^{3,5} \times 4$), 7.01 (8H, t, $H^{3',5'} \times 4$). ^{13}C NMR, δ_C (CD_3CN): 158.50 (8C, $C^{2'6'} \times 4$), 157.46 (8C, $C^{2,6} \times 4$), 137.83 (4C, $C^4 \times 4$), 137.51 (4C, $C^{4'} \times 4$), 126.17 (8C, $C^{3,5} \times 4$), 125.93 (8C, $C^{3'5'} \times 4$). The prime-labeled atoms correspond to the pyridines of the $(NC)Ru^{II}(py)_4(CN)$ fragment. IR (KBr): ν_{CN} (terminal) 2027 (s) cm^{-1}; ν_{CN} (bridge) 2062 (s) cm^{-1}.

***trans*-$[ClRu^{II}(py)_4(NC)Ru^{II}(py)_4(CN)Ru^{II}(py)_4(NO_2)](PF_6)_2$.** A 143.0 mg (0.185 mmol) amount of *trans*-$[Ru^{II}Cl(py)_4(NO)](PF_6)_2$[9] was added to a solution of 12.0 mg of NaN_3 (0.185 mmol) in 15 mL of acetone and allowed to react protected from light at room temperature for 90 min to yield the deep orange solvento complex *trans*-$[Ru^{II}Cl(py)_4(Me_2CO)]^+$.[9] A 200 mg (0.185 mmol) amount of *trans*-$[(NC)Ru^{II}(py)_4(CN)Ru^{II}(py)_4(NO_2)](PF_6)$ previously dissolved in 3.0 mL of acetone was added slowly by means of a gastight syringe, and the resulting solution was allowed to react for 4 days at room temperature in the dark, yielding a deep yellow solution. The crude product was filtered through a 0.45 μm PTFE membrane to remove a small amount of an unidentified precipitate and purified by chromatography using a neutral alumina column (l = 15 cm, ϕ = 4 cm) packed with acetone. Elution with acetone allows removing some unreacted material. Pure acetone leaves the product at the seeding region, but elution with a gradient from 3% to 15% (v/v) of MeOH/acetone develops several yellow fractions that were monitored by UV−vis. The product was mainly contained in the third fraction, which was concentrated to a few milliliters, and treated with water. The product was collected by filtration, washed thoroughly with chilled water, and dried under vacuum. Yield: 43 mg (14%). Anal. Calcd for $C_{62}H_{60}ClF_{12}N_{15}O_2P_2Ru_3$ (MW = 1675.9): C, 44.4; H, 3.6; N, 12.5. Found: C, 44.6; H, 3.7; N, 11.9. ^{1}H NMR, δ_H (CD_3CN): 8.23 (8H, d, $H^{2'',6''} \times 4$), 8.17 (8H, d, $H^{2,6} \times 4$), 7.95 (8H, d, $H^{2',6'} \times 4$), 7.82 (4H, t, $H^4 \times 4$), 7.78 (4H, t, $H^{4'} \times 4$), 7.76 (4H, t, $H^{4''} \times 4$), 7.07 (8H, t, $H^{3,5} \times 4$), 7.02 (8H, t, $H^{3'',5''} \times 4$), 6.88 (8H, t, $H^{3',5'} \times 4$). The prime- and double-prime-labeled atoms correspond to the pyridines of the central $(NC)Ru^{II}(py)_4(CN)$ and terminal $ClRu^{II}(py)_4$ fragments, respectively. IR (KBr): ν(CN) 2071 cm^{-1}. UV−vis (H_2O, pH = 8): $\lambda_{max}(\epsilon)$ 218 nm (45 600 M^{-1} cm^{-1}), 242 nm (42 300 M^{-1} cm^{-1}), 354 nm (41 400 M^{-1} cm^{-1}).

***trans*-$[ClRu^{II}(py)_4(NC)Ru^{II}(py)_4(CN)Ru^{II}(py)_4(NO)](PF_6)_4$ (I).** A 40 mg amount of *trans*-$[ClRu^{II}(py)_4(NC)Ru^{II}(py)_4(CN)Ru^{II}(py)_4(NO_2)](PF_6)_2$ (0.024 mmol) was suspended in 15 mL of water. An aqueous solution of HCl (0.1 M) was added dropwise until the solid dissolved completely, yielding a deep brown solution. This solution was cooled in an ice bath and treated with a saturated solution of NH_4PF_6 in water to yield a brown solid and an almost colorless solution. The precipitate was recovered by filtration, washed with diluted HCl, and vaccuum dried. Yield: 14.0 mg (30%). Anal. Calcd for $C_{62}H_{60}ClF_{24}N_{15}OP_4Ru_3$ (MW = 1949.8): C, 38.2; H, 3.1; N,

(1) (a) Mallah, T.; Thiébaut, S.; Verdaguer, M.; Veillet, P. *Science* **1993**, 1554. (b) Bignozzi, C. A.; Chiorboli, C.; Indelli, M. T.; Scandola, F.; Bertolasi, V.; Gilli, G. *J. Chem. Soc., Dalton Trans.* **1994**, 2391–2395. (c) Entley, W. R.; Girolami, G. S. *Science* **1995**, *268*, 397–400. (d) Balzani, V.; Juris, A.; Venturi, M.; Campagna, S.; S. Serroni, S. *Chem. Rev.* **1996**, 759. (e) Bignozzi, C. A.; Argazzi, R.; Bortolini, O.; Scandola, F.; Harriman, A. *New J. Chem.* **1996**, *20*, 731–738. (f) Bignozzi, C. A.; Schoonover, J. R.; Scandola, F. *Prog. Inorg. Chem.* **1997**, 1. (g) Heintz, K. R. D. a. R. A. *Prog. Inorg. Chem.* **1997**, 283. (h) Vahrenkamp, H.; Geiss, A.; Richardson, G. N. *J. Chem. Soc., Dalton Trans.* **1997**, 3643–3651. (i) Balzani, V.; Campagna, S.; Denti, G.; Juris, A.; Serroni, S.; Venturi, M. *Acc. Chem. Res.* **1998**, 26. (j) Richardson, G. N.; Brand, U.; Vahrenkamp, H. *Inorg. Chem.* **1999**, *38*, 3070–3079. (k) Zhu, N. Y.; Vahrenkamp, H. *J. Organomet. Chem.* **1999**, *573*, 67–72. (l) Chen, Z. N.; Appelt, R.; Vahrenkamp, H. *Inorg. Chim. Acta* **2000**, *309*, 65–71. (m) Geiss, A.; Vahrenkamp, H. *Inorg. Chem.* **2000**, *39*, 4029–4036. (n) Richardson, G. N.; Vahrenkamp, H. *J. Organomet. Chem.* **2000**, *594*, 44–48. (o) Launay, J. P.; Coudret, C. Wires based on metal complexes. In *Electron Transfer in Chemistry*; Balzani, V., Ed.; Wiley-VCH: Weinheim, 2001; Vol. *5*. (p) Appelt, R.; Vahrenkamp, H. *Z. Anorg. Allg. Chem.* **2003**, *629*, 133–138. (q) Albores, P.; Slep, L. D.; Weyhermuller, T.; Baraldo, L. M. *Inorg. Chem.* **2004**, *43*, 6762–6773. (r) Sheng, T. L.; Vahrenkamp, H. *Eur. J. Inorg. Chem.* **2004**, *119*, 8–1203. (s) Vahrenkamp, H.; Sheng, T. *Inorg. Chim. Acta* **2004**, *357*, 1739. (t) Albores, P.; Rossi, M. B.; Baraldo, L. M.; Slep, L. D. *Inorg. Chem.* **2006**, *45*, 10595–10604.

(2) Richter-Addo, G. B.; Legzdins, P. *Metal Nitrosyls*; Oxford University Press: New York, 1992.

(3) Olabe, J. A.; Slep, L. D. Reactivity and Structure of Complexes of Small Molecules: Nitric and Nitrous Oxide. In *Comprehensive Coordination Chemistry II, from Biology to Nanotechnology*; Mc Cleverty, J. A., Meyer, T. J., Eds.; Elsevier: Oxford, 2004; Vol. *1*, pp 603−623.

(4) (a) Enemark, J. H.; Feltham, R. D. *Coord. Chem. Rev.* **1974**, *13*, 339–406. (b) Feltham, R. D.; Enemark, J. H. *Top. Stereochem.* **1981**, 155.

(5) Westcott, B. L.; Enemark, J. H. *Transition Metal Nitrosyls. In Inorganic Electronic Structure and Spectroscopy*; Solomon, E. I., Lever, A. B. P., Eds.; John Wiley & Sons: New York, 1999; Vol. *II*, pp 403−450.

(6) Bottomley, F. In *Reactions of Coordinated Ligands*; Braterman, P. S., Ed.; Plenum: New York, 1989; Vol. *2*.

(7) Roncaroli, F.; Baraldo, L. M.; Slep, L. D.; Olabe, J. A. *Inorg. Chem.* **2002**, *41*, 1930–1939.

(8) Coe, B. J.; Meyer, T. J.; White, P. S. *Inorg. Chem.* **1995**, *34*, 3600–3609.

(9) Coe, B. J.; Meyer, T. J.; White, P. S. *Inorg. Chem.* **1995**, *34*, 593–602.

(10) Bottomley, F.; Mukaida, M. *J. Chem. Soc., Dalton Trans.* **1982**, 1933–1937.

(11) Alessio, E.; Mestroni, G.; Nardin, G.; Attia, W. M.; Calligaris, M.; Sava, G.; Zorzet, S. *Inorg. Chem.* **1988**, *27*, 4099–4106.

(12) Armarego, W. L. F.; Perrin, D. D. *Purification of Laboratory Chemicals*; Reed Educational & Professional Publishing Ltd.: Oxford, 1996.

(13) Kaim, W.; Ernst, S.; Kasack, V. *J. Am. Chem. Soc.* **1990**, *112*, 173.

10.8. Found: C, 37.8; H, 3.2; N, 10.3. ^{1}H NMR, δ_H (CD_3CN): 8.33 (4H, t, $H^4 \times 4$), 8.13 (8H, m, $H^{2'',6''} \times 4$), 8.04 (8H, m, $H^{2,6} \times 4$), 7.89 (12H, m, $H^{4'} \times 4 + H^{2'6'} \times 4$), 7.74 (4H, t, $H^{4''} \times 4$), 7.60 (8H, t, $H^{3,5} \times 4$), 7.02 (16H, m, $H^{3',5'} \times 4 + H^{3'',5''} \times 4$). The prime- and double-prime-labeled atoms correspond to the pyridines of the central (NC)Ru^{II}(py)$_4$(CN) and terminal ClRu^{II}(py)$_4$ fragments, respectively. IR (KBr): ν(CN) 2024 cm^{-1}, ν(NO) 1919 cm^{-1}. UV−vis (CH_3CN) $\lambda_{max}(\epsilon)$: 228 nm (51 100 M^{-1} cm^{-1}), 359 nm (26 330 M^{-1} cm^{-1}), 503 nm (4570 M^{-1} cm^{-1}), 650 nm, sh (2860 M^{-1} cm^{-1}).

Physical Determinations. Microanalytical data for C, H, and N were obtained with a Carlo Erba EA 1108 analyzer. UV−vis spectra were recorded with either an HP8453 or an HP8452A diode array spectrometer. IR spectral measurements (KBr pellets) were carried out using alternatively one of two FT spectrophotometers, a Nicolet 150P and a Thermo Nicolet AVATAR 320. The ^{1}H NMR spectra were measured with a 500 MHz Bruker AM 500 spectrometer; chemical shifts are referred to TMS. For EPR a solution of **I** in MeCN/0.1 M Bu_4NPF_6 was reductively electrolyzed for 5 min at room temperature in a two-electrode capillary cell described elsewhere,[13] leading to a solution of $\mathbf{I_{red}}$. The spectrum was obtained in a glassy frozen solution at 4 K with a Bruker ESP 300 spectrometer equipped with a Bruker gaussmeter ER 35 M and a microwave counter HP5350B. Cyclic voltammetry (CV) measurements were done in acetonitrile (0.1 M Bu_4NPF_6 as supporting electrolyte) with a standard three-electrode cell containing a vitreous carbon electrode (3 mm ∅) and a Pt wire as a counterelectrode. As a reference, a silver wire plus an internal ferrocene (Fc) standard was used.[14] The potential of the working electrode was controlled with a TEQ-03 potentiostat. Spectroelectrochemical experiments yielded solutions of the 1e$^-$ oxidized and 1e$^-$ reduced forms of **I**, *trans*-[ClRu(py)$_4$(NC)Ru(py)$_4$(CN)Ru(py)$_4$(NO)]$^{5+}$ and *trans*-[ClRu(py)$_4$(NC)Ru(py)$_4$(CN)Ru(py)$_4$(NO)]$^{3+}$, $\mathbf{I_{ox}}$ and $\mathbf{I_{red}}$, respectively. The spectroelectrochemical experiments in the UV−vis region were done in a homemade cell containing a quartz cuvette (1 cm path). The potential was controlled with a TEQ-03 potentiostat using either 0.01 M HCl (I = 1 M NaCl) or 0.1 M Bu_4NPF_6 in acetonitrile as supporting electrolyte. A commercial adapted Ag/AgCl reference electrode was used in aqueous solution, whereas a Ag/$AgNO_3$ (0.01 M) electrode was the reference used in organic medium. The working electrode was a Pt net, and a Pt wire was used as the counter electrode. The system was maintained at 25.0 ± 0.1 °C for the experiments in water and −30 ± 1 °C for those in acetonitrile (RC6 LAUDA thermostat) and entirely purged with N_2. Throughout this work all reported redox potentials are referred to AgCl/Ag, 3 M NaCl (0.21 V vs NHE). A typical spectroelectrochemical experiment started with an exhaustive one-electron oxidation to yield $\mathbf{I_{ox}}$ followed by application for a short period of time of a potential sufficiently negative to induce charge circulation at the working electrode. After a short period of time electrolysis was interrupted to allow homogenization of the solution and simultaneous recording of the electronic spectrum and the open-circuit potential of the solution. The redox potentials and disclosed UV−vis spectra of all species present in solution were then obtained by global analysis.[15] The procedure involved a simultaneous multiwavelength fitting assuming that all redox couples behave according to the Nernst equation.[16]

Kinetic studies for addition of OH$^-$ to **I** to yield the nitro species were done under pseudo-first-order conditions at I = 1 M (NaCl). Solutions at different [OH$^-$] were prepared by mixing 1 mL of a ca. 6.31 × 10^{-5} M solution of **I** (0.01 M HCl, I = 1 M, NaCl) with 1 mL of the appropriate ($H_2PO_4^-$/HPO_4^{2-} or $B(OH)_4^-$/$B(OH)_3$) buffer solution (0.33 M, I = 1 M, NaCl) in a 1 cm path length quartz cuvette. For mixtures in which the reaction was completed in less than 5 min, mixing was achieved by a stopped-flow accessory (RX1000 from Applied Photophysics) linked to the diode array spectrometer and provided with a similar quartz cuvette as before. In all cases, the pH was checked after each kinetic run. The pseudo-first-order kinetic constants k_{obs} were obtained by multiwavelength global analysis[15] employing data measured in the UV−vis−NIR range. Plots of k_{obs} vs [OH$^-$] were employed to calculate the second-order rate constant (see text). Rate constants, k_{OH}, at different temperatures (range 20−40 °C) were employed to estimate the activation parameters (enthalpies and entropies) through an Eyring plot, ln (k_{OH}/T) vs 1/T.

Theoretical Calculations. We employed density functional theory (DFT) computations to fully optimize the ground-state geometries of the redox-related cationic species *trans*-[ClRu(py)$_4$(NC)Ru(py)$_4$(CN)Ru(py)$_4$(NO)]$^{5+,4+,3+}$ ($\mathbf{I_{ox}}$, **I**, and $\mathbf{I_{red}}$). The calculations were done with Gaussian 03[17] at the B3LYP level of theory using restricted and unrestricted approximations of the Kohn−Sham equations depending on the total electron counting.[18] In all cases, we employed the effective core potential basis set LanL2DZ, which proved to be suitable for geometry predictions in coordination compounds containing metals of the second row of the transition elements in the Periodic Table. We used tight SCF convergence criteria and default settings in the geometry optimizations.

In the analysis of the electronic structure, including spectral calculation and assignment, we included the solvent treated as a continuum dielectric medium using the PCM approximation as implemented in Gaussian 03.[17]

Results

Synthetic Procedure and Characterization. The compound *trans*-[ClRu^{II}(py)$_4$(NC)Ru^{II}(py)$_4$(CN)Ru^{II}(py)$_4$(NO)](PF$_6$)$_4$ (**I**) can be prepared and isolated in a stepwise fashion which involves two consecutive substitutions in the coordination sphere of the solvento complex *trans*-[Ru^{II}Cl(py)$_4$(Me$_2$CO)]$^+$ to yield the nitro species *trans*-[ClRu^{II}(py)$_4$(NC)Ru^{II}(py)$_4$(CN)Ru^{II}(py)$_4$(NO$_2$)](PF$_6$)$_2$. Addition of acid to an aqueous solutions of the latter induces acid−base changes in the coordinated ligand, yielding the deeply brown colored compound **I** which involves a {RuNO}^{6} moiety (ν_{NO} = 1919 cm^{-1}). A detailed picture of the synthetic strategy is depicted in Scheme 1.

The *trans*-[Ru(py)$_4$] moiety is recognized by its typical ^{1}H NMR signature, consisting of one doublet and two triplets that integrate for 4, 4, and 8 protons, respectively.[8−10] The NMR spectra of *trans*-[(NC)Ru^{II}(py)$_4$(CN)Ru^{II}(py)$_4$(NO$_2$)](PF$_6$) (a species involved in the already reported preparation of *trans*-[(NC)Ru^{II}(py)$_4$(CN)Ru^{II}(py)$_4$(NO)](PF$_6$)$_3$[7] but isolated for the first time in this work) and *trans*-[ClRu^{II}-

(14) Noviandri, I.; Brown, K. N.; Fleming, D. S.; Gulyas, P. T.; Lay, P. A.; Masters, A. F.; Phillips, L. *J. Phys. Chem. B* **1999**, *103*, 6713–6722.
(15) Malinovsky, E. R. *Factor Analysis in Chemistry*, 2nd ed.; Wiley-Interscience: New York, 1991.
(16) (a) Parise, A. R.; Pollak, S.; Slep, L. D.; Olabe, J. A. *An. Asoc. Quim. Argent.* **1995**, *83*, 211–223. (b) Slep, L. D.; Mijovilovich, A.; Meyer-Klaucke, W.; Weyhermuller, T.; Bill, E.; Bothe, E.; Neese, F.; Wieghardt, K. *J. Am. Chem. Soc.* **2003**, *125*, 15554–15570.
(17) Frisch, M. J. et al. *Gaussian 03, Rev. C.02 and D.01*; Gaussian, Inc.: Wallingford, CT, 2004.
(18) Szabo, A.; Ostlund, N. S. *Modern Quantum Chemistry. Introduction Advanced Electronic Structure Theory*, 1st ed.; Dover Publications, Inc.: Mineola, NY, 1989.

Scheme 1. Synthetic Procedures Involved in the Preparation of **I**

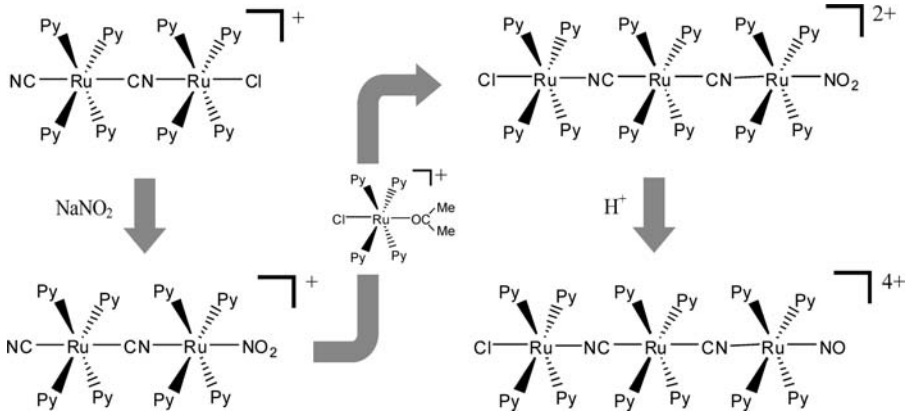

$(py)_4(NC)Ru^{II}(py)_4(CN)Ru^{II}(py)_4(NO_2)](PF_6)_2$ are well resolved and consistent with the presence of two and three *trans*-$[Ru(py)_4]$ units, respectively. Conversion to **I** results in extensive overlap of the signals, which nonetheless allowed us to recognize the linear cyano-bridged backbone that remains unchanged upon acid−base conversion.

The trinuclear compound **I** is stable in acetonitrile. Solutions of this species showed no signs of decomposition after several weeks in dry solvent. The presence of small amounts of water resulted in deterioration of the solutions after a few days. In water, this compound behaves as a typical nitrosyl species displaying the nitrosyl/nitro conversion[3,6,19] as in eq 1

$$[ClRu(py)_4(NC)Ru(py)_4(CN)Ru(py)_4(NO)]^{4+} + 2OH^- \rightleftarrows [ClRu(py)_4(NC)Ru(py)_4(CN)Ru(py)_4(NO_2)]^{2+} + H_2O \quad (1)$$

The reaction proceeds fast enough at pH values higher than 5.0 to allow us to obtain valuable kinetic information. Figure 1 shows the consecutive spectra resulting from addition of the OH^- nucleophile to the coordinated nitrosyl. Consumption of **I** is revealed by the decrease in intensity of the bands in the visible range. Conversion involves well-defined isosbestic points in the UV−visible spectrum, suggesting the presence of only two species: a fact that can be confirmed by factor analysis. The spectrum of the product is completely coincident with that of $[ClRu(py)_4(NC)Ru(py)_4(CN)Ru(py)_4(NO_2)]^{2+}$ measured in an independent experiment. The net process displays a first-order behavior with respect to the concentrations of OH^- and **I** with $k_1 = (12.5 \pm 0.2) \times 10^3$ M^{-1} s^{-1} (25 °C, $I = 1$ M). Determinations at pH = 6.19 and different temperatures yielded the activation parameters $\Delta H^{\ddagger} = 103.8 \pm 1.3$ kJ mol^{-1} and $\Delta S^{\ddagger} = 180.9 \pm 4.1$ J K^{-1} mol^{-1}. Acidification of solutions containing the nitro species down to pH = 1 causes quantitative recovery of **I**.

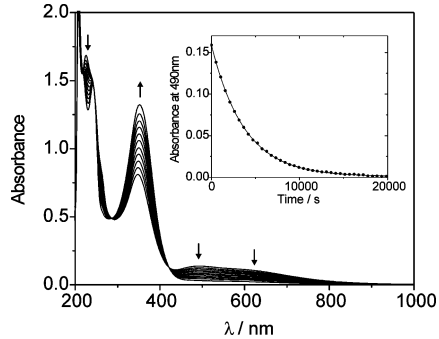

Figure 1. Kinetic data for reaction of **I** with OH^-. $I = 1$ M (NaCl), $T = 25$ °C, $[OH^-] = 1.55 \times 10^{-8}$ M. [Complex] $= 3.16 \times 10^{-5}$ M.

Electrochemistry and Spectroelectrochemistry. The redox properties of **I** were studied by cyclic voltammetry in acetonitrile/0.1 M Bu_4NPF_6. Two redox processes are detectable at 0.71 and 0.51 V vs AgCl/Ag (3 M NaCl), which correspond to the one-electron $\mathbf{I/I_{ox}}$ and $\mathbf{I/I_{red}}$ conversions, respectively. For both processes, the coulometric determinations confirmed the electron count as described above. The redox processes were also studied by spectroelectrochemistry in the same solvent (0.71 and 0.49 V). Figure 2a shows the UV−vis−NIR spectra associated with the $\mathbf{I_{ox}} \rightarrow \mathbf{I} \rightarrow \mathbf{I_{red}}$ redox conversions. Global analysis confirms the absence of any other absorbing species. The electrochemical oxidation/reduction experiments are fully reversible, and solutions of these species at any oxidation level are stable for several hours in the absence of oxygen. Global analysis also renders the spectra of the various species and confirms the redox potentials for the different redox couples (see the Experimental Section for details on the methodology). The disclosed individual spectra are displayed as insets in Figure 2a, while the absorption maxima, extinction coefficients, and redox potentials for the different species are summarized in Table 1. Among the most remarkable changes, one can notice the complete disappearance of the absorption pattern observed for **I** in the visible range upon reduction and its replacement by new bands at 481 and 846 nm upon oxidation. The cyclic voltammetry experiments in acetonitrile show that $\mathbf{I_{ox}}$ can be further oxidized at much higher potentials (1.69 V). The highly charged (+6) species proved to be very sensitive to small amounts of water. This is not totally unexpected as our previous experience had indicated that the electrophilicity of the nitrosyl moiety increases upon oxidation of the distant Ru centers.[7] The instability of this molecule precluded an appropriate characterization by spectroelectrochemistry as performed for the other oxidation states. The redox properties of **I** were also explored in water. To prevent complications derived from the acid−base interconversion the experiments

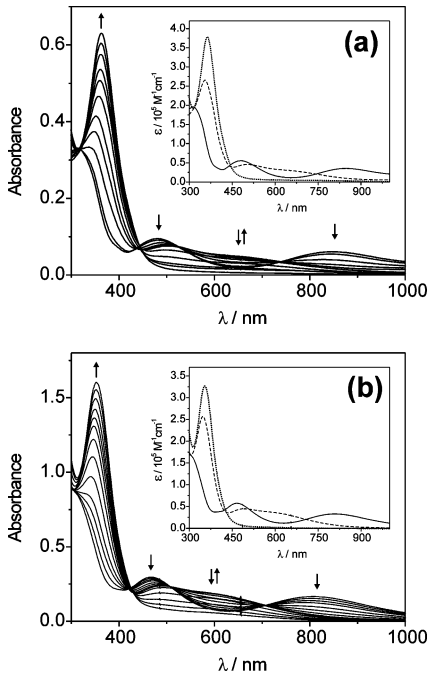

Figure 2. $\mathbf{I_{ox}} \rightarrow \mathbf{I} \rightarrow \mathbf{I_{red}}$ redox conversion under controlled potential conditions: **(a)** Acetonitrile/0.1 M Bu_4NPF_6, **(b)** Aqueous HCl 0.01 M, $I =$ 1 M (NaCl), [complex] $= 1.7 \times 10^{-5}$ M and 5.3×10^{-5} M for acetonitrile and water, respectively. The arrows indicate the spectral changes upon reduction. Inset: Deconvoluted spectra for $\mathbf{I_{red}}$ (dotted line), **I** (dashed line), and $\mathbf{I_{ox}}$ (full line) obtained by factor analysis (see text).

Table 1. UV−Vis−NIR and Electrochemical Results (Acetonitrile and Aqueous Solutions) for *trans*-[ClRu^{II}(py)$_4$(NC)Ru^{II}(py)$_4$(CN)Ru^{II}(py)$_4$(NO)]$^{5+,4+,3+}$ ($\mathbf{I_{red}}$, **I**, and $\mathbf{I_{ox}}$)

	λ_{max} (ϵ), nm (M^{-1} cm^{-1})		$E°$, V[b]	
complex	H_2O[a]	MeCN	H_2O[a]	MeCN
$\mathbf{I_{red}}$	242 (49 440)	246 (53 300)		
	265sh (31 360)	265sh (27 750)		
	288sh (25 790)	289 (23 600)	0.20[c]	0.49[c]
	354 (32 850)	364 (37 820)		
I	228 (57 200)	228 (51 100)		
	242sh (50 450)	246 (46 500)		
	262sh (28 400)	264sh (25 400)		
	348 (26 900)	359 (26 330)	0.57[c]	0.71[c]
	490 (4480)	503 (4570)		
	600sh (3600)	650sh (2860)		
$\mathbf{I_{ox}}$	260 (47 150)	257 (47 300)		
	313 (16 210)	313 (19 610)		1.69[d]
	465 (5750)	481 (5540)		
	808 (3290)	846 (3530)		

[a] 0.01 M HCl ($I = 1$ M NaCl). [b] Against AgCl/Ag, 3 M NaCl. [c] Obtained from spectroelectrochemical experiments. [d] CV, 0.02 V/s, in acetonitrile/ 0.1 M Bu_4NPF_6.

were performed at pH = 2. The spectral changes during the spectroelectrochemical experiments shown in Figure 2b are very similar to those described in CH_3CN and indicative of two one-electron reduction processes at 0.57 and 0.20 V which correspond to the one-electron $\mathbf{I/I_{ox}}$ and $\mathbf{I/I_{red}}$ conversions, respectively. In spite of some small but detectable shifts of the UV−vis−NIR bands, the electronic spectra of the different species retain their general appearance (Table 1), suggesting that the redox chemistry in water parallels the one observed in acetonitrile.

EPR Spectrum of $\mathbf{I_{red}}$. In order to explore the nature of the one-electron-reduced $\mathbf{I_{red}}$ species we collected an X-band

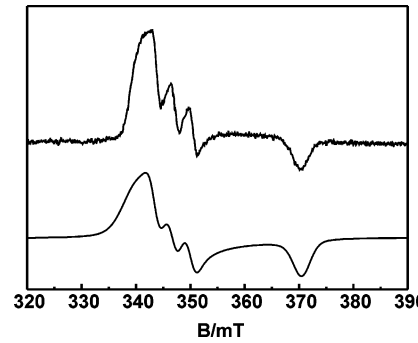

Figure 3. (top) EPR spectrum of the electrogenerated cation [ClRu^{II}(py)$_4$(NC)Ru^{II}(py)$_4$(CN)Ru^{II}(py)$_4$(NO)]$^{3+}$ ($\mathbf{I_{red}}$) in MeCN/0.1 M Bu_4NPF_6 at 4 K and (bottom) computer simulated spectrum (see parameters in the text).

EPR spectrum of this species at 4 K in frozen acetonitrile. For this experiment the sample was electrogenerated and rapidly frozen. Figure 3 shows the obtained spectrum together with the results of the powder simulation, which required considering the hyperfine coupling with one nitrogen nucleus (^{14}N, 99.64% natural abundance, $I = 1$). The least-squares fitting parameters resulted in the following spin Hamiltonian parameters: $g = 2.028$, 1.990, 1.862 and $A_2(^{14}N) = 33$ G. These features are in line with other reports on coordinated NO$^{\bullet}$,[7,20,21] including ruthenium complexes, and will be discussed later.

DFT Calculations. Analysis of the electronic structure of the species presented in this report may profit from structural information. In spite of our efforts we were unable to collect single crystals suitable for X-ray analysis of the compounds described here. To compensate for this we carried out DFT-based calculations that included computation of the optimized geometries of the three nitrosyl species described here (**I**, $\mathbf{I_{red}}$, and $\mathbf{I_{ox}}$) at the B3LYP/LanL2DZ level of theory. This approach provides not only structural parameters (bonds and angles) but also valuable information which in conjunction with the spectroscopic results helps to understand the electronic structure of the trinuclear compounds. Figure 4 displays the optimized

(19) Olabe, J. A. *Adv. Inorg. Chem.* **2004**, *55*, 61–126.
(20) (a) Callahan, R. W.; Meyer, T. J. *Inorg. Chem.* **1977**, *16*, 574–581. (b) Sarkar, S.; Sarkar, B.; Chanda, N.; Kar, S.; Mobin, S. M.; Fiedler, J.; Kaim, W.; Lahiri, G. K. *Inorg. Chem.* **2005**, *44*, 6092–6099. (c) Mondal, B.; Paul, H.; Puranik, V. G.; Lahiri, G. K. *J. Chem. Soc., Dalton Trans.* **2001**, 481–487. (d) Chanda, N.; Paul, D.; Kar, S.; Mobin, S. M.; Datta, A.; Puranik, V. G.; Rao, K. K.; Lahiri, G. K. *Inorg. Chem.* **2005**, *44*, 3499–3511. (e) Chanda, N.; Mobin, S. M.; Puranik, V. G.; Datta, A.; Niemeyer, M.; Lahiri, G. K. *Inorg. Chem.* **2004**, *43*, 1056–1064. (f) Wanat, A.; Schneppensieper, T.; Stochel, G.; van Eldik, R.; Bill, E.; Wieghardt, K. *Inorg. Chem.* **2002**, *41*, 4–10. (g) Westre, T. E.; Di Cicco, A.; Filipponi, A.; Natoli, C. R.; Hedman, B.; Solomon, E. I.; Hodgson, K. O. *J. Am. Chem. Soc.* **1994**, *116*, 6757–6768. (h) Brown, C. A.; Pavlosky, M. A.; Westre, T. E.; Zhang, Y.; Hedman, B.; Hodgson, K. O.; Solomon, E. I. *J. Am. Chem. Soc.* **1992**, *114*, 9189–9191. (i) Sellmann, D.; Blum, N.; Heinemann, F. W.; Hess, B. A. *Chem. Eur. J.* **2001**, *7*, 1874–1879.
(21) (a) McGarvey, B. R.; Ferro, A. A.; Tfouni, E.; Bezerra, C. W. B.; Bagatin, I.; Franco, D. W. *Inorg. Chem.* **2000**, *39*, 3577–3581. (b) Serres, R. G.; Grapperhaus, C. A.; Bothe, E.; Bill, E.; Weyhermuller, T.; Neese, F.; Wieghardt, K. *J. Am. Chem. Soc.* **2004**, *126*, 5138–5153. (c) Li, M.; Bonnet, D.; Bill, E.; Neese, F.; Weyhermuller, T.; Blum, N.; Sellmann, D.; Wieghardt, K. *Inorg. Chem.* **2002**, *41*, 3444–3456. (d) Wanner, M.; Scheiring, T.; Kaim, W.; Slep, L. D.; Baraldo, L. M.; Olabe, J. A.; Zalis, S.; Baerends, E. J. *Inorg. Chem.* **2001**, *40*, 5704–5707. (e) Frantz, S.; Sarkar, B.; Sieger, M.; Kaim, W.; Roncaroli, F.; Olabe, J. A.; Zalis, S. *Eur. J. Inorg. Chem.* **2004**, *290*, 2–2907.

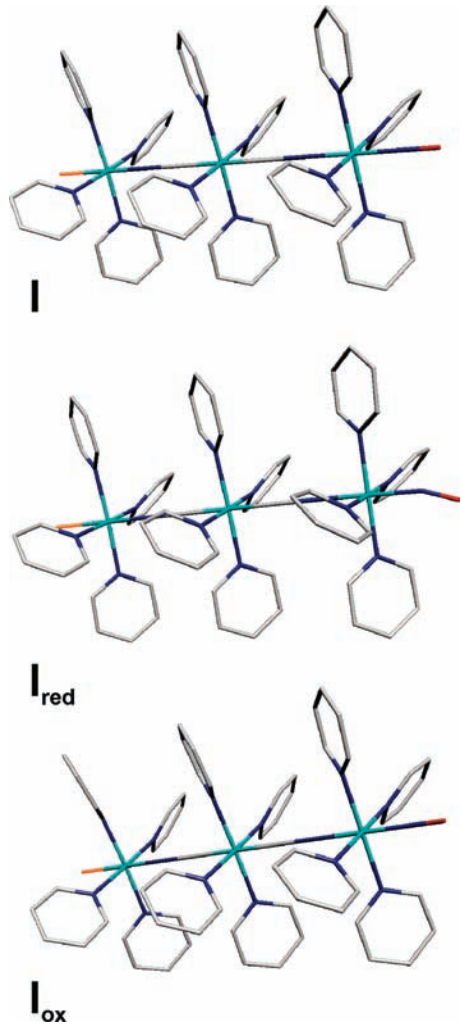

Figure 4. Optimized geometry of **I**, $\mathbf{I_{red}}$, and $\mathbf{I_{ox}}$ at the DFT/B3LYP level of theory.

geometries for the different species; some relevant bond lengths and angles are summarized in Table 2.

The computed structure for **I**, $\mathbf{I_{red}}$, and $\mathbf{I_{ox}}$ share the following features: (a) Almost perfectly colinear arrangements of the nine atoms Cl−Ru−N−C−Ru−C−N−Ru−N with a total length of ca. 14.9 to 15.9 Å for the backbone of the structures. (b) Three $Ru(py)_4$ complex fragments are obtained which show the classical paddle-wheel disposition of the pyridine molecules with tilting angles in the range of 38−47°. (c) A completely eclipsed arrangement of the pyridine ligands of the different moieties was computed as the energy minimum.

Apart from these general features the following specific geometrical and electronic characteristics should be noted: (a) The Ru−N−O fragment in **I** is linear with Ru−N and N−O bond lengths of 1.819 and 1.197 Å, respectively. (b) The {Ru−NO} group does not bend on oxidation to $\mathbf{I_{ox}}$, maintaining a Ru−N−O angle of 180.0° and Ru−N and N−O distances of 1.781 and 1.181 Å, respectively. On the contrary, the optimized structure of the one-electron-reduced $\mathbf{I_{red}}$ reveals a bent Ru−N−O arrangement (143.5°) with significantly elongated Ru−N and N−O distances (1.889 and 1.223 Å, respectively). (c) The computed spin density of $\mathbf{I_{ox}}$ is fully located on the terminal $[ClRu(py)_4]$ fragment, while it is delocalized on the $[Ru(py)_4(NO)]$ fragment in the case of $\mathbf{I_{red}}$(Figure 5).

Table 2. Significant Structural Parameters (bond distances and angles) As Obtained from the DFT Geometry Optimization for $\mathbf{I_{red}}$,, and $\mathbf{I_{ox}}$ in Vacuo[a]

distance	$\mathbf{I_{red}}$ (Å)	**I** (Å)	$\mathbf{I_{ox}}$ (Å)	**II** (Å)[c]
$Cl-Ru_a$	2.490	2.440	2.375	2.422
Ru_a-N	2.069	2.058	2.132	2.012
N−C	1.993	1.195	1.192	1.158
$C-Ru_b$	2.086	2.080	2.109	2.040
Ru_b-C	2.056	2.029	2.031	
C−N	1.197	1.205	1.205	
$N-Ru_c$	2.139	2.045	2.055	
Ru_c-N	1.889	1.819	1.781	
N−O	1.223	1.197	1.181	
Ru_a-Npy[b]	2.122	2.133	2.144	2.078
Ru_b-Npy[b]	2.142	2.152	2.159	2.092
Ru_c-Npy[b]	2.144	2.150	2.156	2.078
Ru_a-Ru_b	5.348	5.333	5.433	5.209
Ru_b-Ru_c	5.391	5.278	5.291	5.209
Ru_a-Ru_c	10.740	10.611	10.725	10.416
angle	$\mathbf{I_{red}}$ **(deg)**	**I (deg)**	$\mathbf{I_{ox}}$ **(deg)**	**II (deg)**
$Cl-Ru_a-N$	180.0	180.0	180.0	177.6
$C-Ru_b-C$	179.9	180.0	180.0	177.5
$N-Ru_c-N$	179.2	180.0	180.0	
Ru_c-NO	143.5	180.0	180.0	
$N-Ru_c-Cl$				177.6
$Cl-Ru_a-Npy$[b]	88.1	88.0	88.5	90.3
$C-Ru_b-Npy$[b]	89.1	88.8	88.8	90.0
$N-Ru-Npy$[b]	90.3	90.1	90.0	89.7

[a] Relevant parameters for the closest experimentally studied structure $[ClRu^{II}(py)_4(NC)Ru^{II}(py)_4(CN)Ru^{II}(py)_4Cl]^{2+}$ **(II)** are also included for comparison. [b] Mean values. [c] Values taken from ref 8.

Discussion

Basic Characterization and Electrophilic Reactivity. The synthetic steps involved in preparation of **I** rely on use of *trans*-$[Ru^{II}Cl(py)_4(NO)](PF_6)_2$, a valuable precursor that combines ease of preparation with two different axial ligands that undergo stepwise substitution to afford *trans*-heterosubstituted compounds.[8,9] The key step involves reaction of $[Ru^{II}Cl(py)_4(Me_2CO)]^+$ (prepared in situ by treating the nitrosyl species with NaN_3)[9] and $[(NC)-Ru^{II}(py)_4(CN)Ru^{II}(py)_4(NO_2)]^+$ in deaerated acetone under mild conditions to yield $[ClRu^{II}(py)_4(NC)Ru^{II}(py)_4(CN)Ru^{II}(py)_4-(NO_2)]^{2+}$ (Scheme 1). The impurities that develop along the reaction can be effectively eliminated by chromatography before conversion to the final nitrosyl stage. This last step is performed in acidified water, from which $[ClRu^{II}(py)_4(NC)Ru^{II}(py)_4(CN)Ru^{II}-(py)_4(NO)]^{4+}$ (**I**) can be isolated as a PF_6^- salt. We avoided the alternative pathway that involves use of the highly charged $[(NC)Ru^{II}(py)_4(CN)Ru^{II}(py)_4(NO)]^{3+}$ instead of the dinuclear nitro precursor. Under these latter conditions the reaction proceeded extremely slowly and led to a mixture of products that suggested redox interactions between the oxidizable solvento monomer and the easily reducible nitrosyl species ($E° = 0.50$ V in acetonitrile).[9]

In spite of the lack of an X-ray crystal structure characterization, the well-known reactivity of the fragments employed in the synthesis complemented with the NMR spectroscopic information leave no doubt concerning the linear nature of the trimetallic arrangement. The presence of the nitrosyl moiety is revealed by its IR stretching frequency ($\nu_{NO} = 1919$ cm^{-1}). This experimental ν_{NO} is

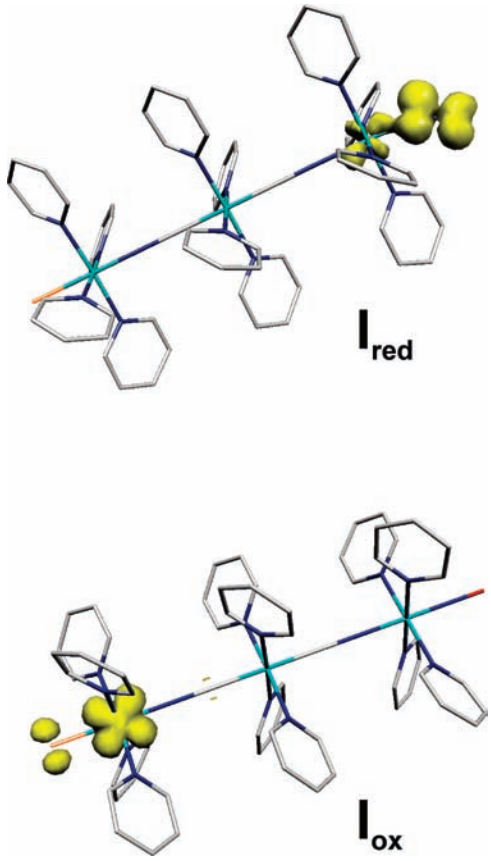

Figure 5. Computed spin density (DFT/B3LYP) for $\mathbf{I}_{red}$ and $\mathbf{I}_{ox}$.

essentially identical to the one of the related $[(NC)Ru^{II}(py)_4(CN)Ru^{II}(py)_4(NO)]^{3+}$ (1920 cm^{-1}, KBr pellet)[7] and comparable to those reported for other hexacoordinated $\{MNO\}^6$ species.[3,4] $\{RuNO\}^6$ complexes with ν_{NO} values in the range of 1800−2000 cm^{-1} are customary described as possessing an essentially $Ru^{II}-NO^+$ electronic distribution. This description is also favored by DFT computations.

Geometry optimization (Figure 4) shows a fully linear arrangement of the metal centers, a linear Ru−N−O fragment, and a paddle-wheeled disposition of the pyridine coligands to yield a molecule with almost perfect C_4 symmetry with three metal centers and the nitrosyl aligned along the principal axis. A relevant collection of geometrical parameters is presented in the Results section. The closest experimentally studied structure is that of $[ClRu^{II}(py)_4(NC)Ru^{II}(py)_4(CN)Ru^{II}(py)_4Cl]^{2+}$.[8] Some relevant parameters for the latter are also included for comparison in Table 2. It becomes evident at first sight that the DFT computed distances of **I** are consistently longer (up to 0.08 Å depending on the particular bond) than those found experimentally in the dichloride compound. This effect could hardly be ascribed to the intrinsic differences between both compounds and is most probably due to the computational methodology. In fact, the bond lengths in ECP-DFT (effective core potential) geometries obtained at this level of theory are usually slightly overestimated.[22,23]

The DFT information allows us to gain some insight into the electronic distribution in the $\{RuNO\}^6$ fragment of **I**. Specifically, the Ru−N and N−O bond lengths at 1.819 and 1.197 Å and the Ru−N−O angle of 180.0° are consistent with an electronic distribution close to the limiting $Ru^{II}-NO^+$ case, in agreement with the vibrational spectroscopy analysis.

Deviations from an idealized C_4 geometry in **I** are small, and this point group can be safely assumed for the qualitative analysis of the electronic structure of this species. Under C_4 symmetry the octahedral $d_\pi(t_{2g})$ sets at the three metal centers split into $e(d_{yz}, d_{xz})$ and $b(d_{xy})$. The degeneracy of the $d_\sigma(e_g)$ set is also lifted with the individual orbitals transforming as $a(d_{z^2})$ and $b(d_{x^2-y^2})$. The $d_\pi(b)$ of the different metal centers are too far apart from each other, making any interaction negligible. On the contrary, the $d_\pi(e)$ orbitals are properly oriented to interact with empty and filled chloro-, cyano-, and nitrosyl-centered orbitals of the same symmetry to generate an extended π-backbone along the molecular axis.

A single-point DFT computation in acetonitrile (PCM approximation, see the Experimental Section for details) reveals that the degenerate HOMO orbitals (297/298) are mostly located on the $[ClRu(py)_4]^+$ side of the molecule with noticeable contributions from the $[(NC)Ru(py)_4(CN)]$ fragment and a minor percentage of $[Ru(py)_4NO]^{3+}$ character (92%, 6%, and 2% of orbitals of the three complex fragments, respectively). The LUMO orbitals (299/300) lie ca. 5×10^3 cm^{-1} higher in energy and are complementary centered on the opposite side of the molecule with 2%, 11%, and 87% relative contributions from the same fragments. The next metal-centered $d_\pi(e)$ orbitals (293/294) are stabilized by ca. 10×10^3 cm^{-1} and comprise 90% $[(NC)Ru(py)_4(CN)]$ character and minor contributions (3% and 7%) of $[ClRu(py)_4]^+$ and $[Ru(py)_4(NO)]^{3+}$ orbitals, respectively (see Supporting Information, Figure S1). This picture reveals a partial delocalization of the π-electronic density from the electron-rich chloro fragment to the distant nitrosyl *mediated* by the central dicyanoruthenium moiety. The amount of π density transferred to the nitrosyl by this mechanism is only moderate, in agreement with the relatively high ν_{NO} stretching frequency.

The low energy of the nitrosyl-centered LUMO becomes experimentally evident in the electrophilic reactivity of this species. Reaction of **I** with OH^- is first order in both reactants with a second-order rate constant of $k_1 = 12.5 \pm 0.2 \times 10^3$ M^{-1} s^{-1} (25 °C, $I = 1$ M) (Figure 1). This reaction proceeds by a well-studied mechanism described by eqs 2, 3 and 4.

$$[M-NO]^{x+} + OH^- \rightleftarrows \{[M-NO]^{x+} \cdots OH^-\} \quad K_{ip} \quad (2)$$

$$\{[M-NO]^{x+} \cdots OH^-\} \rightleftarrows [M-NO_2H]^{(x-1)+} \quad k_3, k_{-3} \quad (3)$$

$$[M-NO_2H]^{(x-1)+} + OH^- \rightleftarrows [M-NO_2]^{(x-2)+} + H_2O \quad K_4 \quad (4)$$

For sufficiently high $[OH^-]$ this mechanism yields the rate law $v = K_{ip}k_3[[M-NO]^{x+}]\cdot[OH^-]$. The second-order rate constant reflects both the electrophilicity of the species and the ion-pairing tendency between the complex and the hydroxyl ion. A proper comparison between different species requires an estimation of K_{ip}. This can be roughly done by

(22) Roncaroli, F.; Ruggiero, M. E.; Franco, D. W.; Estiu, G. L.; Olabe, J. A. *Inorg. Chem.* **2002**, *41*, 5760–5769.

means of an electrostatic model.[24] For the case of **I**, we estimate K_{ip} as 3.3 M^{-1}, and therefore, $k = 3.8 \times 10^3$ M^{-1} s^{-1}. This value is essentially identical to the one reported in $[(NC)Ru^{II}(py)_4(CN)Ru^{II}(py)_4(NO)]^{3+}$,[22] showing that once the charge effects have been accounted for the electrophilicity of $\{RuNO\}^6$ is very similar in both compounds.

Electronic Spectroscopy and Spectroelectrochemistry. The UV region of the spectrum of **I** in acetonitrile solution is dominated, as in other $Ru(py)_4$ containing species, by the intraligand $\pi \rightarrow \pi^*$ transition at ca. 250 nm and the $d_\pi(t_{2g}) \rightarrow \pi^*(py)$ transition at 359 nm, arising from several metal centers (Table 1 and Figure 2a). Apart from these characteristics which are also observable in the individual fragments that compose this species two partially overlapped intense aborptions dominate the visible region of the spectrum. A Gaussian deconvolution analysis of the absorption profile in this region uncovers two bands centered at 501 ($\nu_{max} = 20.0 \times 10^3$ cm^{-1}, $\Delta\nu_{1/2} = 4425$ cm^{-1}, $f_{osc} = 0.078$) and 650 nm ($\nu_{max} = 15.4 \times 10^3$ cm^{-1}, $\Delta\nu_{1/2} = 5980$ cm^{-1}, $f_{osc} = 0.077$). A similar treatment of the absorption spectrum in water also yields two bands at 478 ($\nu_{max} = 20.9 \times 10^3$ cm^{-1}, $\Delta\nu_{1/2} = 4505$ cm^{-1}, $f_{osc} = 0.076$) and 605 nm ($\nu_{max} = 16.5 \times 10^3$ cm^{-1}, $\Delta\nu_{1/2} = 5660$ cm^{-1}, $f_{osc} = 0.086$).

Reduction of **I** leads (as with $[(NC)Ru^{II}(py)_4(CN)Ru^{II}(py)_4(NO)]^{3+}$) to complete disappearance of these features. EPR and computational evidence point to a nitrosyl-centered reduction that involves considerable geometry changes, particularly bending of the Ru−N−O angle and lengthening of the N−O bond (Figure 4 and Table 2). In glassy frozen solution the X-band EPR spectrum of $\mathbf{I_{red}}$ (see Figure 3) shows the typical pattern associated to the $\{RuNO\}^7$ systems (rhombic g matrix with ^{14}N hyperfine coupling noticeable for the central component).[21] This pattern reflects the high degree of covalency of the Ru−N bond in the bent Ru−NO. The total spin anisotropy $\Delta g = 0.161$ is the highest reported among the series of $\{RuNO\}^7$ systems, including $[(NC)Ru^{II}(py)_4(CN)Ru^{II}(py)_4(NO)]^{2+}$ ($\Delta g = 0.159$). The large spin anisotropy probably reflects, as already reported in the dinuclear species, the effect of the large spin−orbit coupling constant of the other metal centers. The DFT computations support this argument: the majority of the spin density is concentrated (98%) on the $[Ru(py)_4(NO)]^{2+}$ side of the molecule (Figure 5). The remaining 2% density is calculated at the neighboring $[(NC)Ru(py)_4(CN)]$, and virtually no spin density is delocalized to the chlororuthenium side of the molecule.

The discoloration that follows the $\mathbf{I} \rightarrow \mathbf{I_{red}}$ ($\{RuNO\}^6 \rightarrow \{RuNO\}^7$) redox conversion is a strong indication that the $\{RuNO\}^6$ fragment behaves, as in $[(NC)Ru^{II}(py)_4(CN)Ru^{II}(py)_4(NO)]^{3+}$, as the acceptor partner in charge-transfer processes.

As evident from its molecular orbital structure, **I** is well suited for intramolecular charge transfer. The occurrence of two bands in the visible region suggests the possibility of two z-polarized electronic transitions that involve donor orbitals of e symmetry located on two different neighboring metal centers. The high-energy component at 501 nm in acetonitrile solution (478 nm in water)[25] can be associated with the charge transfer involving the dicyanoruthenium fragment as the donor center. This transition shows a relative blue shift with respect to the analogous dinuclear species because of the stabilization of the d_π orbitals in $[(NC)Ru(py)_4(CN)]$ upon coordination of the positively charged moiety. The low-energy component might in turn arise from the distant $[ClRu(py)_4]^+$. The intensity of the close and distant transitions are comparable, an observation that has already been reported in mixed-valent D−A triads.[26] Individually they are less intense than that the donor−acceptor charge-transfer (DACT) band in $[(NC)Ru^{II}(py)_4(CN)Ru^{II}(py)_4(NO)]^{3+}$ ($f_{osc} = 0.150$ and 0.151 in acetonitrile and water, respectively), but combined they account for roughly the same total intensity. This suggests an intensity stealing mechanism which results from the extensive orbital mixing of the $[ClRu(py)_4]^+$ and $[(NC)Ru(py)_4(CN)]$ fragments.

Oxidation under controlled potential conditions leads to $\mathbf{I_{ox}}$, which shows important spectral changes, particularly in the visible−NIR. The high-energy band shifts to 481 nm in acetonitrile ($\nu_{max} = 20.7 \times 10^3$ cm^{-1}, $\Delta\nu_{1/2} = 6105$ cm^{-1}, $f_{osc} = 0.156$) and 465 nm in water ($\nu_{max} = 21.5 \times 10^3$ cm^{-1}, $\Delta\nu_{1/2} = 5770$ cm^{-1}, $f_{osc} = 0.153$). The low-energy band is replaced by a weaker absorption at 846 ($\nu_{max} = 11.8 \times 10^3$ cm^{-1}, $\Delta\nu_{1/2} = 3870$ cm^{-1}, $f_{osc} = 0.063$) or 808 nm ($\nu_{max} = 12.4 \times 10^3$ cm^{-1}, $\Delta\nu_{1/2} = 3910$ cm^{-1}, $f_{osc} = 0.059$) for acetonitrile and water, respectively. The DFT-optimized structure for this species is consistent with a Ru-centered oxidation that occurs on the chloro end of the molecule. The computed spin density is localized at this end of the molecule (98%) with marginal spin polarization over the dicyano moiety. The unpaired electron (see Figure 5) is in a $d_\pi(e)$ orbital.

This electronic configuration allows for two CT transitions involving the central $[(NC)Ru(py)_4(CN)]$ as the donor partner and either end of the molecule as electron acceptors, consistent with the observed experimental spectrum. A simple comparison with the position, intensity, and shape of the spectrum of $[(NC)Ru^{II}(py)_4(CN)Ru^{II}(py)_4(NO)]^{3+}$ suggests that the high-energy band (blue shifted due to the electron-withdrawing properties of the Ru(III) fragment) arises from a $d_\pi(e) \rightarrow e(\{RuNO\}^6)$ CT transition. The low-energy component becomes in turn a typical intervalence CT involving the neighboring cyanide-bridged Ru^{II}/Ru^{III} fragments.

Conclusions and Perspectives

The species described in this manuscript contribute to the growing reports on the D−A charge-transfer spectroscopy

(23) (a) Li, J.; Noodleman, L.; Case, D. A. Electronic Structure Calculations: Density Functional Methods with Applications to Transition Metal Complexes. In *Inorganic Electronic Structure and Spectroscopy*; Solomon, E. I., Lever, A. B. P., Eds.; John Wiley & Sons: New York, 1999; Vol. *I*, p 661; (b) Videla, M.; Jacinto, J. S.; Baggio, R.; Garland, M. T.; Singh, P.; Kaim, W.; Slep, L. D.; Olabe, J. A. *Inorg. Chem.* **2006**, *45*, 8608–8617.

(24) Fuoss, R. M. *J. Am. Chem. Soc.* **1958**, *80*, 5059–5061.

(25) The maxima reported here arise from a Gaussian deconvolution performed over the experimental absorption profile in order to obtain the area of the overlapping bands. For this reason the numbers differ slightly form those reported in Table 1.

(26) (a) von Kameke, A.; Tom, G. M.; Taube, H. *Inorg. Chem.* **1978**, *17*, 1790–1796. (b) Macatangay, A. V.; Endicott, J. F. *Inorg. Chem.* **2000**, *39*, 437–446.

Scheme 2. Redox States and Spectroscopic Properties

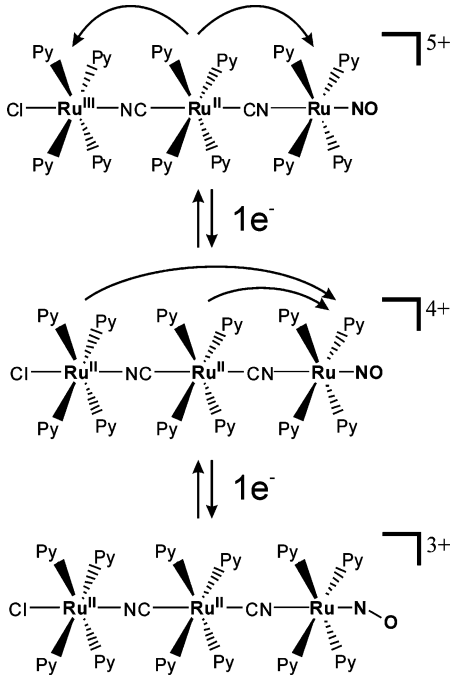

of trinuclear systems, which frequently involve mixed-valent species. The redox-related **I**, $\mathbf{I_{red}}$, and $\mathbf{I_{ox}}$ can be efficiently converted into each other with significant changes in their electronic and spectroscopic properties. Scheme 2 summarizes the electronic description for these species according to simultaneous analysis of the experimental and computational information performed in this work.

Previous work revealed the origin of a single intense visible band in *trans*-[(NC)Ru^{II}(py)$_4$(CN)Ru^{II}(py)$_4$(NO)]$^{3+}$ as arising from a donor−acceptor charge-transfer process between mildly coupled centers. Although the Robin and Day classification scheme[27] was originally developed for mixed-valent species, in this description the donor [(NC)Ru^{II}(py)$_4$(CN)] and acceptor [Ru^{II}(py)$_4$(NO)]$^{3+}$ moieties could be described as the complementary fragments of a Class II partially delocalized species. The new all-*trans*-[ClRu^{II}(py)$_4$(NC)Ru^{II}(py)$_4$(CN)Ru^{II}(py)$_4$(NO)]$^{4+}$ roughly preserves the spectroscopy of its dinuclear parent but shows a second transition at lower energies and in this sense can be also thought as a Class II species of a higher level. The spectroscopic evidence at different redox stages allowed us to assign the transitions in **I** as arising from the neighboring and distant Ru^{II} donor fragments, in agreement with the electronic structure picture derived from the DFT computations. Both **I** and $\mathbf{I_{ox}}$ are good examples that demonstrate that the {RuNO}^{6} moiety can behave as an acceptor partner not only in D−A dyads but also in systems of higher nuclearity, giving rise to rich DACT spectroscopy, which is a direct consequence of the electronic interactions between orbitals of the different fragments that constitute an extended π backbone.

As a bonus, the electrophilic reactivity of the {RuNO}^{6} fragment is well preserved, making both extremes in *trans*-[ClRu^{II}(py)$_4$(NC)Ru^{II}(py)$_4$(CN)Ru^{II}(py)$_4$(NO)]$^{4+}$ potentially susceptible to controlled substitution by different fragments, something that cannot be achieved with the related [ClRu^{II}(py)$_4$(NC)Ru^{II}(py)$_4$(CN)Ru^{II}(py)$_4$Cl]$^{2+}$.[8] The robustness displayed by **I** throughout this work coupled to the presence of the space-demanding pyridines suggest that the linear configuration would not be lost in further synthetic steps. Moreover, it is possible to think of variations that incorporate substituted pyridines into the Ru^{II} coordination spheres. All these perspectives turn species of this kind into attractive precursors for larger and more complex structures and eventually for design of new molecular wires; we are currently exploring such extensions.

Acknowledgment. The authors thank the University of Buenos Aires (UBA), the Consejo Nacional de Investigaciones Científicas y Técnicas (CONICET), the Agencia Nacional de Promoción Científica y Tecnológica (ANPCyT) and Fundación Antorchas (Argentina), as well as the Deutsche Forschungsgemeinschaft (Germany) for funding. This work was partially supported by the National Center for Supercomputing Applications under grant TG-MCA05S010. L.D.S. is a member of the scientific staff of CONICET, and A.G.D. is a graduate fellow from UBA.

Supporting Information Available: Relevant molecular orbitals obtained for **I** (DFT, B3LYP/LanL2DZ). This material is available free of charge via the Internet at http://pubs.acs.org.

IC801347D

(27) Robin, M. B.; Day, P. *Adv. Inorg. Chem. Radiochem.* **1967**, *10*, 247.